Nanoimprinted Polymer Solar Cell

Yi Yang,[†] Kamil Mielczarek,[‡] Mukti Aryal,[⊥] Anvar Zakhidov,[†,‡] and Walter Hu[†,§,*]

[†]Department of Materials Science and Engineering, [‡]Department of Physics, and [§]Department of Electrical Engineering, The University of Texas at Dallas, Richardson, Texas 75080, United States, and [⊥]Rolith Inc., Pleasanton, California 94588, United States

ABSTRACT Among the various organic photovoltaic devices, the conjugated polymer/fullerene approach has drawn the most research interest. The performance of these types of solar cells is greatly determined by the nanoscale morphology of the two components (donor/acceptor) and the molecular orientation/crystallinity in the photoactive layer. A vertically bicontinuous and interdigitized heterojunction between donor and acceptor has been regarded as one of the ideal structures to enable both efficient charge separation and transport. Synergistic control of polymer orientation in the nanostructured heterojunction is also critical to improve the performance of polymer solar cells. Nanoimprint lithography has emerged as a new approach to simultaneously control both the heterojunction morphology and polymer chains in organic photovoltaics. Currently, in the area of nanoimprinted polymer solar cells, much progress has been achieved in the fabrication of nanostructured morphology, control of molecular orientation/crystallinity, deposition of acceptor materials, patterned electrodes, understanding of structure—property correlations, and device performance. This review article summarizes the recent studies on nanoimprinted polymer solar cells and discusses the outstanding challenges and opportunities for future work.

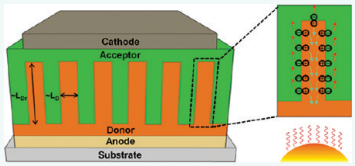

KEYWORDS: polymer solar cells · conjugated polymers · nanoimprint lithography · nanoscale morphology · phase separation · nanostructure geometry · chain alignment · charge carrier mobility · interface · manufacture

In recent years, photovoltaic (PV) technology, which harvests energy directly from sunlight, is being increasingly recognized as an essential component for future global energy production. Among existing solar cells, organic photovoltaics (OPVs) have many favorable characteristics, such as the potential of being flexible, semitransparent, and applicable to low-cost manufacturing processes such as screen-printing, inkjet, and roll-to-roll.[1,2] As an important member of the OPV family, polymer solar cells draw the most research interest, due to the relatively high power conversion efficiency (PCE) achieved when compared to other types of OPVs such as small-molecule solar cells.[3−5] However, compared to the high efficiencies (>10%) of inorganic solar cells, the best polymer solar cells (6−7%) still show a lower efficiency.[6,7] Two critical factors limiting the performance of OPVs are the short exciton diffusion length (~10 nm) and low mobility of charge carriers, especially the hole mobility ($\mu_h \sim 10^{-6}$−10^{-3} $cm^2 \cdot V^{-1} \cdot s^{-1}$) within the photoactive layer.[8−14] The bulk heterojunction (BHJ) structure has greatly improved the efficiency of polymer solar cells due to the formation of a large donor/acceptor interface, allowing for more efficient exciton dissociation.[15−17] However, the active layer morphology within this structure still remains disordered and far from ideal. The discrete and randomly distributed phases cause significant charge recombination, as well as a significant amount of disorder in the polymer chains resulting in low carrier mobility.[18] Further improvements of OPV performance can be achieved through new techniques which result in a more favorable active layer morphology and an increase in exciton dissociation rates as well as charge carrier transport.[19]

Many of the above-mentioned problems can be addressed if a vertically bicontinuous and interdigitized heterojunction nanomorphology as shown in Figure 1 can be achieved. The simulation work from Verschoor *et al.* has suggested that a similar morphology enabled as much as 80% internal quantum efficiency, in comparison to 15% for most BHJ blends,[18] indicating a possible 5-fold improvement in PCE. Forrest *et al.* have observed that the external quantum efficiency of OPVs obtained by this morphology was the highest compared to other counterparts, such as bilayer or blend structures.[20] The nanoscale interdigitized morphology decouples absorption depth and charge transport channels from the diffusion length, allowing for highly efficient lateral exciton diffusion and vertical charge transport with reduced recombination rates.

Despite the previously mentioned advantages of a vertically bicontinuous and interdigitized heterojunction, finding a practical means of achieving this morphology remains a fundamental challenge. Many different

* Address correspondence to walter.hu@utdallas.edu.

Received for review January 11, 2012 and accepted March 2, 2012.

Published online March 06, 2012
10.1021/nn3001388

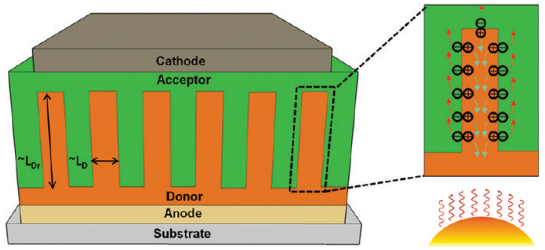

Figure 1. Schematic of the ideal bicontinuous and interdigitated donor–acceptor bulk heterojunction polymer solar cell. The phase separation between donor and acceptor is within the exciton diffusion length (L_D), allowing for efficient exciton dissociation. The height is greater than 50% of the photon mean free path but within the drift length (L_{Dr}) of charge carriers for both sufficient light absorption and charge collection. The thin layers of pure donor and acceptor close to anode and cathode, respectively, prevent charge carrier recombination. Ideal molecule arrangement (not shown) within donor and acceptor and at their interface which assists exciton dissociation and charge transport is equally important.

methods such as polymer nanowires, nanoparticles, block copolymers, layer-by-layer deposition, nanoimprint lithography (NIL), template methods, nanoelectrodes, and porous inorganic materials have been studied and reviewed to make nanostructured organic solar cells.[21,22] Among them, NIL is seen as an emerging technique which can define such morphologies due to its high patterning resolution, high-throughput, and good fidelity as proven in the literature.[23–25] Besides the enhanced donor/acceptor interface and exciton dissociation, it has been found that charge carrier transport in conjugated polymers can be enhanced by NIL-induced polymer chain alignment.[26–28] Better light trapping within the active layer by NIL has been reported by different groups and summarized elsewhere.[29] Improved light absorption and charge collection have been observed in devices with inorganic and organic electrodes patterned by this technique, as well.[30,31] With significant progress achieved in the field, NIL has become a new and promising technique to produce highly efficient OPVs.

It is worth noting that, in previous works of nanoimprinted OPVs, there were large variations of specific fabrication methods, materials used, and processing details. For example, various donor and acceptor materials were chosen and processed differently. Moreover, various nanostructure geometries of molds have been used to fabricate imprinted OPVs, resulting in different sizes and shapes of donor/acceptor junctions which in turn affected the device performance. Due to these experimental variations, it is difficult to compare one work with another to validate the methods and underlying science. Currently, the fundamental understanding of structure–performance correlations of nanoimprinted OPVs is still quite limited. For instance, contradicting observations of polymer chain orientation and mobility enhancement in nanoimprinted

VOCABULARY: polymer solar cells – solar cells based on conjugated polymers as the active layer; **nanoimprint lithography** – an approach to fabricate nanoscale patterns by the mechanical deformation of imprint resist and other following processes; **active layer morphology** – the overall form of active layer structure, including crystallinity, roughness, phase, molecular weight, and so on; **phase separation** – separation of material regions which are chemically uniform and physically dissimilar; **chain alignment** – process by which polymer molecules aggregate together to form an ordered region; **mobility** – term to describe how fast electrons or holes can move in metals or semiconductors under a certain electric field;

poly(3-hexylthiophene) (P3HT) nanostructures have been reported by different groups,[27,28,32,33] indicating that a complete understanding of chain alignment and crystallinity by nanoimprint is not yet established.

To develop a comprehensive understanding of nanoimprinted OPVs, it is important to review recent work on this type of solar cell. In this paper, we first summarize what has been achieved in the field of nanoimprinted OPVs. We review and compare different nanoimprint lithographic techniques employed to fabricate nanoimprinted OPVs in literature. Then we discuss the geometric effects of imprinted nanostructures on device performance. The effects of nanoimprint on polymer chain alignment and its influence on charge transport are reviewed. The progress on electrode patterning for polymer solar cells is introduced, as well. Finally, the current challenges and future tasks for nanoimprinted OPVs are previewed. The goal of this review is to help develop a better understanding of nanoimprinted OPVs so as to unleash the full potential of this emerging technique toward significant improvements of OPV performance.

Fabrication. *Nanoimprinted Polymer Solar Cells.* The general process flow for NIL is given in Figure 2a,b. Typically, a nanostructured mold treated with an antiadhesion layer such as a 1*H*,1*H*,2*H*,2*H*-perfluorodecyltrichlorosilane (FDTS) monolayer is brought into contact with the polymer to be imprinted. Under a certain applied pressure and temperature, the polymer in the viscous state flows into the cavities of the mold and forms nanostructures. For nanoimprinted polymer solar cells, this temperature is important and usually set to be ~50 °C higher than the polymer's glass transition temperature (T_g), which changes the polymer from a rigid solid state into a viscous state and helps its flowing during imprinting.[25] Before demolding, the system is cooled down while maintaining the applied pressure in order to prevent polymer reflow. Finally, the mold is released from the sample, and polymer nanostructures with negative replication of the mold are formed. Figure 2c,d shows the scanning electron microscopic (SEM) images of a Si nanograting mold

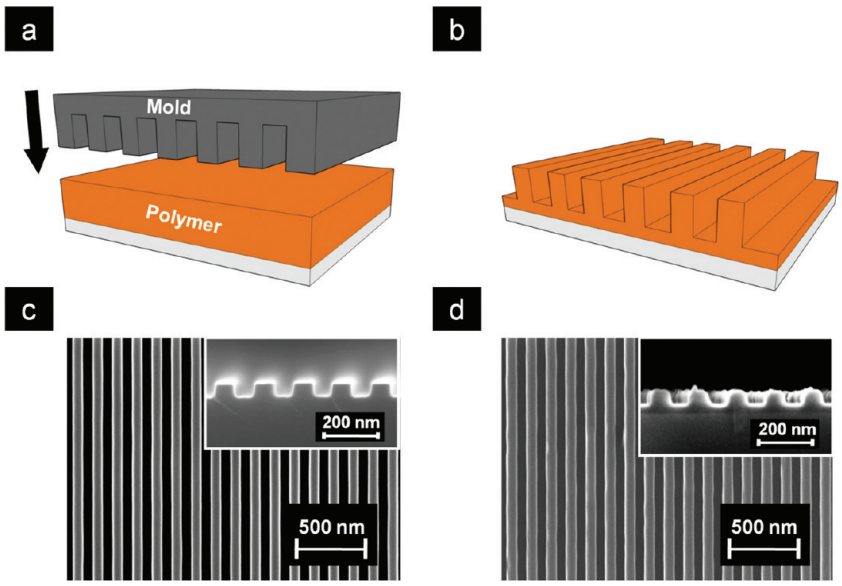

Figure 2. Process flow of the thermal nanoimprint lithography: schematic of (a) a mold is pressed onto a thin layer of polymer on a substrate heated to a temperature above the polymer's glass transition temperature, and (b) polymer nanostructures of negative replication to the mold are formed after demolding. SEM images of (c) Si nanolined mold and (d) imprinted P3HT nanogratings.

and imprinted P3HT nanogratings. It can be seen that the nanostructures on Si mold are transferred into P3HT film with excellent fidelity.

For the nanoimprinted solar cells to obtain high performance, the complete infiltration of acceptor materials into the nanostructured donor polymer layer is critical in order to form an intimate and large interfacial area junction for efficient exciton dissociation, charge separation, and collection. To date, three typical acceptor deposition methods are widely used in literature: (a) spin-coating,[34,35] (b) physical vapor deposition,[36,37] and (c) double nanoimprint or lamination.[38,39] The choice of which method to use is primarily based on the properties of donor and acceptor materials within the device.

In order to use spin-coating to deposit acceptor materials onto imprinted donor nanostructures, two main requirements must be satisfied: (a) the solvent used for the acceptor solution needs to be orthogonal; that is, it only dissolves the acceptor material but not the donor, otherwise the nanostructure formed by NIL can be dissolved or damaged; (b) the solvent must wet the donor materials so that the acceptor material can spread uniformly over and into the nanostructures. With the efforts of many groups, some proper solvents have been developed to spin-coat specific acceptors onto the imprinted donor nanostructures. For example, dichloromethane (DCM) has been demonstrated as a proper solvent for spin-coating [6,6]-penyl-C61-butyric acid methyl ester (PCBM) onto the nanoimprinted P3HT structures to form P3HT/PCBM OPVs.[34,40] As shown in Figure 3a1,a2, Aryal *et al.* have demonstrated that DCM was a suitable solvent to spin-coat PCBM while allowing for complete infiltration of PCBM into P3HT nanogratings.[28] The complete filling of PCBM into P3HT nanostructures using DCM as a solvent has also been shown by Wiedemann *et al.*, where they employed grazing-incidence small-angle X-ray scattering (GISAXS) to characterize the PCBM coverage into P3HT nanostructures.[35] However, Avnon *et al.* have observed that DCM could slightly dissolve P3HT and decrease the height (~10%) of imprinted P3HT nanostructures.[41] To understand these contradicting observations, we studied the solubility of P3HT in DCM with different molecular weights (MW) and found that DCM dissolves low MW ($M_n \sim 13K$), partially dissolves medium MW ($M_n \sim 20K$), but does not dissolve high MW ($M_n \sim 25K$) P3HT. Therefore, high MW P3HT is desirable for spin-coating with DCM and can be obtained by extraction methods such as soxhlet extraction. Besides DCM for PCBM spin-coating, Sellinger *et al.* employed 2-butanone as solvent for 4,7-bis(2-(1-ethylhexyl-4,5-dicyanoimidazol-2-yl)vinyl)benzo-[*c*]1,2,5-thiadiazole (EV-BT) to successfully fabricate nanoimprinted P3HT/EV-BT solar cells.[42]

Spin-coating has been proven as an effective, simple, and low-cost process to fill acceptor materials into imprinted donor materials. However, for some acceptors which have very low solubility in common solvents, or for which orthogonal solvents cannot be found, spin-coating is not feasible. In many cases, finding orthogonal solvents can be challenging because good donor and acceptor materials for organic solar cells are originally designed and synthesized to show similar solving behavior so that a bulk heterojunction structure can be realized. To overcome the drawbacks of spin-coating, physical vapor deposition (PVD) can be used as an alternative method to deposit acceptor materials in nanoimprinted solar cells. As the

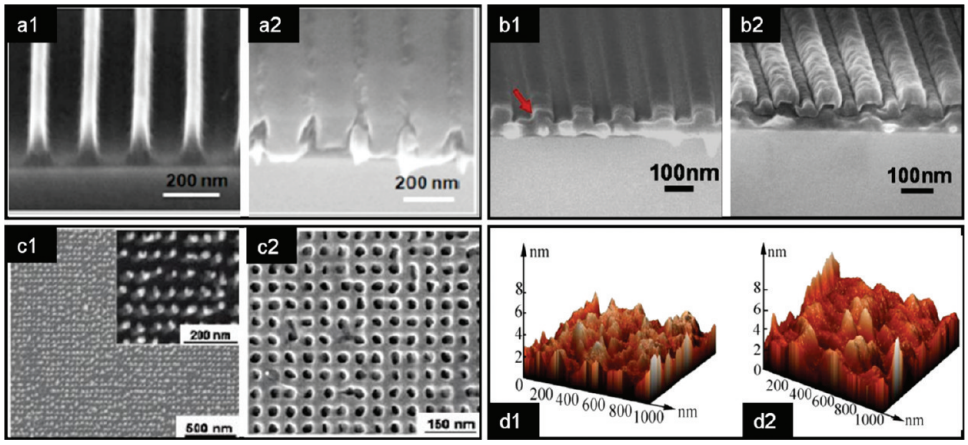

Figure 3. Summary of active layer patterning by NIL. (a) Spin-coating: P3HT nanogratings (a1) before and (a2) after PCBM spin-coating. (b) Thermal evaporation: P3HT nanogratings with C_{60} coated (b1) from one direction where only one wall is covered (shown by arrow) and (b2) from both direction for complete coverage. (c) Double nanoimprint: (c1) 25 nm nanodots in P3HT imprinted by Si mold and (c2) holes in F8TBT imprinted by P3HT nanodots. (d) P3HT:PCBM blend: (d1) before and (d2) after direct patterning. Images (a, b) reprinted with permission from refs 28, 37. Copyright 2010 American Institute of Physics. Image (c) reprinted from ref 38. Copyright 2010 American Chemical Society. Image (d) reprinted with permission from ref 48. Copyright 2009 American Institute of Physics.

most popular method in PVD, thermal evaporation is widely used in OPV fabrication. The challenge of complete filling of acceptors into donor nanostructures with this method arises from the poor step coverage (little coating on the sidewalls), especially when donor nanostructures have a high aspect ratio. An oblique angle deposition is employed to overcome this problem.[43] In Figure 3b1,b2, it is shown that using oblique angle thermal evaporation of C_{60} into P3HT nanogratings from both sides separately can result in complete C_{60} filling into P3HT nanogratings.[37] To improve acceptor coverage into imprinted nanostructures, instead of thermal evaporation, gas-transport-based organic vapor phase deposition was employed by Heremans *et al.* as a more isotropic deposition method to deposit *N,N′*-ditridecyl-3,4,9,10-perylenetetracarboxylic diimide (PTCDI-C_{13}) into P3HT trenches.[36] Complete coverage of PTCDI-C_{13} onto P3HT was achieved by this method. Despite these achievements mentioned above, some limitations exist for the fabrication of imprinted OPVs using this method. For example, typically a high vacuum is required for PVD, making this method more costly and slower. In addition, PVD is difficult to realize for materials which do not have the required vapor pressure for evaporation, such as conjugated polymer acceptors.

Recently, there has been a third method to fabricate nanoimprinted OPVs using lamination reported by He *et al.*[38,39] In their first work, with solvent vapor-assisted nanoimprint, P3HT was initially patterned by a Si mold under room temperature, and the patterned nanostructures were used as mold to imprint the acceptor poly((9,9-dioctylfluorene)-2,7-diyl-*alt*-[4,7-bis(3-hexylthien-5-yl)-2,1,3-benzothiadiazole]-2′,2″-diyl) (F8TBT).[38] Therefore, one of the requirements for this lamination technique is that the first imprinted polymer be mechanically strong. Figure 3c1,c2 shows images of 25 nm nanodots in P3HT imprinted by Si mold and holes in F8TBT imprinted by P3HT nanodots. This solvent-assisted double imprinting technique provides a low-cost way to make nanoimprinted OPVs with donors and acceptors having an intimate contact with one another. Double nanoimprinted P3HT/PCBM and F8TBT/PCBM solar cells using this lamination technique have also been reported in their later work, demonstrating this technique's wide application.[39]

Nanoimprinted Blend Solar Cells. In literature, most nanoimprinted OPVs have architectures where fullerene acceptors were infiltrated into nanoimprinted polymer nanostructures. However, some studies have shown that NIL could also be used to pattern the blended active layer in polymer solar cells directly to improve the device performance. The improvement is attributed to increased active layer roughness by NIL, causing light scattering at the interface between active layer and metal electrode to be enhanced, and thus leading to increased light absorption and photocurrent.[44,45] Device performance can also be improved because hydrostatic pressure during imprinting increases the crystallinity and mobility of organic semiconductors by decreasing the intermolecular spacing.[46,47] In the work from Li *et al.*, a ~50% increase in PCE was observed in nanoimprinted P3HT:PCBM BHJ solar cells.[48] Figure 3d1,d2 shows the atomic force microscopic (AFM) images of blended P3HT:PCBM solar cells before and after patterning; a clear increase in roughness by NIL can be observed. The enhanced light-trapping ability was responsible for a higher short circuit current (J_{sc}). The largest improvement in device performance was an increase in fill factor (FF) attributed to nanoimprint-induced molecular ordering of the P3HT, which was qualitatively verified by their Raman study on the effects of pressure on the P3HT:PCBM active layer.

The positive effect of nanoimprint lithography on blended P3HT:PCBM solar cells was also reported by Lee *et al.*[49] In their work, the P3HT:PCBM blended solar cells were imprinted by an anodic aluminum oxide (AAO) mold, which could be used as a cost-effective and simple method for mold fabrication. Patterned devices showed a 25% increase in PCE. The increase was mainly due to an improved J_{sc} and attributed to increased utilization as a result of scattering as verified by their reflectance study and an improved crystalline ordering of the P3HT domain as confirmed by their grazing-incidence X-ray diffraction (GIXRD) study.

Geometric Effect. Increases in the donor/acceptor interfacial area by NIL can be quantified by the interface enhancement factor (IEF); its value is determined by the nanostructure's specific geometries. For instance, for nanogratings with height h, width w, and spacing p, IEF can be expressed as eq 1, while for nanopillars with pitch d, radius r, and height h, IEF can be calculated approximately by eq 2.[35,37]

$$\mathrm{IEF} = 1 + \frac{2h}{w+p} \quad (1)$$

$$\mathrm{IEF} = \frac{(2\pi rh + d^2)}{d^2} \quad (2)$$

Theoretically, the donor/acceptor interfacial area increase in imprinted devices compared to a planar interface (*i.e.*, IEF) is determined by the aspect ratio and density of nanostructures. Therefore, to improve the exciton dissociation, nanostructures with a higher IEF are desired. Through simulation, Wiedenmann *et al.* found that the J_{sc} for nanoimprinted P3HT:PCBM solar cells were proportional to the interfacial area between P3HT and PCBM.[50] Kim *et al.* found that, besides width/spacing, the thickness of imprinted nanostructures was also important and needed to be optimized according to the photon mean free path.[51] They concluded that, in the optimum design, the nanostructure size and spacing must be 2−3 times smaller than the exciton mean diffusion length and the active layer thickness should be greater than 50% of the photon mean free path for sufficient light absorption. Besides these simulation studies, a great deal of experimental work has been carried out to study the geometric effect of nanostructures on OPV performance, as summarized in Table 1. The first experimental study on the geometric effects was reported from Kim *et al.*[52] In their work, two different molds with the same height (200 nm) but different periods (510 and 700 nm) resulting in different IEFs were used to imprint the thermally deprotectable polythiophene derivative (TDPTD) donor layer to fabricate nanoimprinted TDPTD/PCBM solar cells. They found that, as the donor/acceptor interfacial area increased, the J_{sc} increased. Also in the work from Cheyns *et al.*, the positive effect of nanostructures with large IEFs was observed from nanoimprinted P3HT/PTCDI-C_{13} solar cell.[36] Recently, He *et al.* systemically studied the geometric effect of nanostructures on imprinted P3HT/F8TBT solar cell performance by using molds of different sizes.[38] Both external quantum efficiency (EQE) and J_{sc} increased with A/A_0 (A, interfacial area of imprinted layer; A_0, interfacial area of initial nonimprinted layer). Also these parameters increased with the decrease of nanostructure width. The smallest feature they made (height h was fixed at 75−80 nm, but width w and spacing p were decreased to 25 nm) yielded the best performance. In their later work, they found the same trends for F8TBT/PCBM and P3HT/PCBM solar cells made by this double imprint technique.[39] Of particular interest is that the highest PCE achieved in P3HT/PCBM solar cells was up to 3.25% when the smallest feature was used, and this is the highest reported efficiency for imprinted P3HT/PCBM solar cells to date.

Effects on Chain Alignment and Charge Transport. For organic solar cells, it is fundamentally important to achieve control of favorable molecular orientation and crystallinity for efficient charge transport.[53] Not only is the overall crystallinity of the conjugated polymers important, but the conductivity in each direction is equally critical in determining charge transport. For example, the charge carrier mobility in P3HT is inversely proportional to the charge carrier's hopping distance. Therefore, the hole mobility is higher ($\sim$0.1 $cm^2 \cdot V^{-1} \cdot s^{-1}$) along the $\pi-\pi$ stacking and backbone directions, with relatively short hopping distance b ($\sim$0.38 nm) and c ($\sim$0.38 nm), than along the hexyl side chain direction (10^{-10} $cm^2 \cdot V^{-1} \cdot s^{-1}$), with long hopping distance a ($\sim$1.69 nm), as shown in Figure 4a.[32,53−57] In most P3HT-based OPVs, where the active layer is vertically sandwiched between anode and cathode, it is preferable for P3HT chain alignment to be perpendicular to the substrate, that is, in face-on or vertical orientations. Annealing the device at temperatures higher than the T_g of P3HT has been shown to allow the polymer chains to reorder in a more thermodynamically favorable way and increase its crystallinity.[58−60] However, it is evident that, under annealing, P3HT thin films tend to be aligned parallel to the substrate, that is, in edge-on orientation, and thus limit the vertical conductivity.[55,56,61,62]

Recently, NIL has proven to be an effective way to crystallize polymers such as polyvinylidene fluoride (PVDF) and poly(9,9-dioctylfluorene-*co*-benzothiadiazole) (F8BT) with controlled orientations.[26,63−66] For P3HT, this NIL-induced polymer chain ordering has been confirmed by different groups. For example, Cui *et al.* used polarizing microscopy to characterize P3HT thin films and found that there were obvious differences in optical birefringence in imprinted P3HT grating images, as compared to nonimprinted areas that underwent the same thermal treatment. This indicated a preferred chain orientation in patterned P3HT thin

TABLE 1. Performance Summary of Photovoltaic Devices with Different Geometries (width w, spacing p and height h) in Literature[a]

reference	donor/acceptor	structure	feature size width (nm)	dimension notes	A/A_0	V_{oc} (V)	J_{sc} (mA/cm^2)	FF	PCE (%)
52	TDPTD/PCBM	planar			1	0.78	0.58	0.34	0.25
		nanograting	520/180	w/p, h=200 nm	1.57	0.78	1	0.47	0.66
			380/130		1.80	0.78	1.19	0.48	0.80
36	P3HT/PTCDI-C13	planar			1.00	0.406	0.32	0.53	0.070
		nanograting	70/70	w/p/h	1.50	0.98	0.45	0.53	0.096
			50/50		1.70	0.390	0.48	0.55	0.104
			50/50		3.00	0.220	0.74	0.25	0.040
38	P3HT/F8TBT	planar			1.00	1.06	0.94	0.39	0.36
		blend			N/A	1.12	2.32	0.42	1.09
		2D dot array	200	w=p, h=80 nm	1.45	1.08	1.81	0.39	0.77
			150		1.60	1.12	1.99	0.39	0.87
			100		1.90	1.14	1.96	0.43	0.97
			80		2.00	1.14	2.35	0.43	1.14
			40		3.67	1.13	2.79	0.47	1.48
			25		4.20	1.14	3.30	0.49	1.85
39	F8TBT/PCBM	planar			1.00	1.00	1.61	0.24	0.38
		blend			N/A	1.01	4.78	0.39	1.90
		nanograting	50/50	w/p, h=80 nm	2.60	1.04	2.83	0.28	0.82
			20/80		2.60	1.04	3.13	0.28	0.92
		2D dot array	200	w=p, h=80 nm	1.45	1.09	3.44	0.28	1.05
			150		1.60	1.08	4.09	0.28	1.23
			100		1.90	1.14	4.15	0.29	1.35
			80		2.00	1.14	4.26	0.35	1.69
			40		3.67	1.18	4.49	0.39	2.04
			25		4.20	1.17	4.99	0.39	2.30
39	P3HT/PCBM	planar			1.00	0.62	4.51	0.49	1.36
		blend			N/A	0.65	9.18	0.59	3.50
		blend (air)			N/A	0.63	8.57	0.59	3.20
		nanograting	50/50	w/p, h=80 nm	2.60	0.62	5.52	0.53	1.82
			20/80		2.60	0.61	5.97	0.55	2.01
		2D dot array	200	w=p, h=80 nm	1.45	0.62	6.49	0.49	1.96
			150		1.60	0.61	7.14	0.54	2.35
			100		1.90	0.61	7.61	0.58	2.65
			80		2.00	0.64	7.72	0.57	2.84
			40		3.67	0.64	7.92	0.59	2.97
			25		4.20	0.64	8.65	0.56	3.25

[a] Table reprinted with permission from the references as indicated. Copyright 2008 IOPscience (ref 36). Copyright 2010 American Chemical Society (ref 38). Copyright 2011 John Wiley and Sons (ref 39). Copyright 2007 American Institute of Physics (ref 52).

films, which was confirmed by X-ray diffraction (XRD) study.[27] To further study this chain alignment by nanoimprint confinement, we performed both out-of-plane and in-plane grazing-incidence XRD (GIXRD) on imprinted P3HT nanogratings and nanopillars.[32] It was shown that a vertical chain alignment in P3HT can be achieved in imprinted P3HT nanostructures compared to the edge-on orientation in nonimprinted films. It was believed that this chain alignment was due to thermal dynamical vertical flow of polymers in the nanocavities and the interaction between the hydrophobic side chains of P3HT and the hydrophobic surface of the mold (treated with hydrophobic FDTS).[62]

Recently, the NIL-induced chain alignment in P3HT nanostructures was also studied by Hlaing *et al.*[33] However, instead of observing vertical alignment, their work found a face-on orientation in P3HT nanogratings. To understand these contradicting studies and also general molecular orientation of nanoimprinted nanostructures, it is important to understand how polymers flow into the mold cavities during NIL. Many studies have shown that the polymer flow during NIL can be strongly affected by the geometries of the mold cavity such as widths, heights, and residual layer thicknesses, which may result in different polymer chain orientations. For instance, the effect of nanostructure width on P3HT chain alignment has been systematically studied by McGehee *et al.*[67] In their study, P3HT nanopillars with the same height (~300 nm) but different widths (20−120 nm) were made by filling the polymer into anodic alumina film with different pore diameters. They found that the ratio of out-of-plane ($\alpha_\perp$) to in-plane ($\alpha_\parallel$) absorption coefficients, $\alpha_\perp/\alpha_\parallel$, increased with a decrease of P3HT nanopillar width, indicating that the polymer chains were more oriented in the vertical direction within narrow P3HT nanopillars.

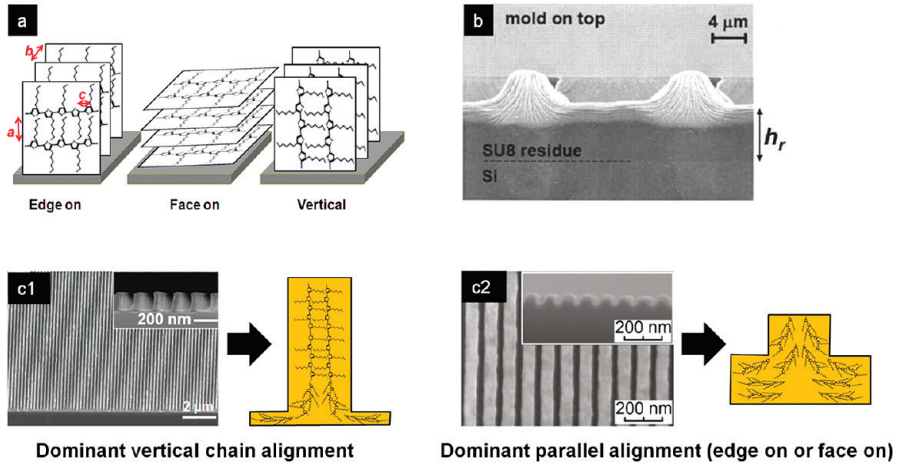

Figure 4. (a) Schematic of edge-on, face-on, and vertical orientation of P3HT chains on substrate. (b) Cross-sectional SEM image of SU-8 gratings with "rippling" patterns formed by partially curing SU-8 with UV light on purpose before the nanoimprint. (c) SEM images of imprinted P3HT nanostructures with different geometries and schematic of their effects on chain alignment/orientations: (c1) dominant vertical chain alignment in 200 nm height and 20 nm residual layer and (c2) the dominant parallel chain alignment in 50 nm height and 75 nm residual layer P3HT nanograting. (Height and residual layer thickness are calculated from ref 33.) Images (a, c1) reprinted from ref 32. Copyright 2009 American Chemical Society. Image (b) reprinted with permission from ref 68. Copyright 2007 American Institute of Physics. Image (c2) reprinted from ref 33. Copyright 2011 American Chemical Society.

They believed that the reason for the preferred vertical alignment in narrow nanostructures was that, when the polymer flowed into the nanopores, the rod-like polymer chains were too rigid to lie horizontally within the narrow pores. Our previous work on polymer flow characterization demonstrated the movement of SU-8 polymers into mold cavities during imprint, which was visualized by partially UV curing the SU-8 before imprint.[68] As shown in Figure 4b, the rippling patterns of SU-8 that were formed during NIL indicate how a linear polymer would align in the imprinted structure: parallel within the residual layer of SU-8, tilted on the corner between nanostructures and residual layer, and vertical when flowing into the cavity. Here we apply these general polymer flow behaviors during NIL to analyze the previously reported chain alignment in imprinted P3HT nanostructures.[32,33] It is reasonable to speculate that the ratio of each orientation (vertical and parallel) in the P3HT nanostructure is dependent on the height and/or aspect ratio of nanostructures, that is, more vertical alignment than parallel alignment in higher nanostructures. In addition, the XRD results also reveal the chain alignment within the residual layer, which is most likely parallel in the film (*i.e.*, edge-on or face-on) if it is not negligible compared to the height of nanostructures. Therefore, the residual layer thickness can affect the XRD results and the conclusion of chain orientation. Huck *et al.* have shown that, for the conjugated polymer F8BT, the NIL-induced ordering started from the surface of the mold and progressively vanished when going further into the residual film.[26,64] Hu *et al.* have shown that for polymers like PVDF a full chain alignment within the patterned nanostructures could only happen at full confinement, that is, no residual layer beneath the nanostructures.[63,66] On the basis of the above-mentioned literature studies of NIL-induced chain alignment and the fundamental studies of polymer flow in NIL, it appears that the molecular orientation induced by NIL can be greatly affected by the geometry of nanostructures, including width, height, aspect ratio, residual layer thickness, and molecular weight of polymer.

To explain the contradiction between the results of our group and those of Ocko's group, we provide two examples based on findings observed in literature. As shown in Figure 4c1, the first example consists of imprinted P3HT nanostructures having large height but small width or high aspect ratio, similar to our work (in which P3HT nanogratings having width $w = 65$ nm, height $h = 200$ nm, and residual layer thickness $r = 20$ nm were characterized). The second example, as shown in Figure 4c2, is similar to that from Ocko *et al.*, where they studied P3HT nanostructures with comparable width $w = 60-70$ nm (measured from figure in literature), yet small height $h = 50$ nm and large residual layer thickness $r > 50$ nm (calculated from literature). It can be seen that the vertical orientation is likely dominant in our imprinted nanostructures because P3HT molecules fully flow into the deep mold cavity. Additionally, due to the thin residual layer in our work, the observed XRD signal is mainly from the imprinted nanostructure. Recently, we have reconfirmed these measurements, showing the presence of vertical alignment and absence of the face-on orientation (results not shown). In the work of Ocko *et al.*, it is likely that P3HT molecules were only partially aligned due to the limited movement within the shallow mold cavity, making the face-on orientation

dominant. The thick residual layer might contribute to the total XRD signal, as well, resulting in a conclusion of face-on orientation. It is worth noting that all of these statements are based on results reported in literature and our speculation. To confirm our statements experimentally, we are currently investigating such effects by systematically studying chain orientations for P3HT nanostructures with varied widths, heights, residue thicknesses, and molecular weights.

The importance of understanding and controlling polymer orientation in nanostructures stems from the strong effects of molecular ordering on carrier mobility in the direction of photocurrent flow. The effect of this nanoimprint-induced chain alignment on μ_h in P3HT has been confirmed by previous work in nanoimprinted P3HT-based organic field effect transistors (OFETs).[27,28] Field effect transistors were fabricated using these nanogratings, and device measurements showed a 60-fold hole mobility enhancement, as compared to that of nonimprinted thin film transistors.[28] Cui *et al.* also found a 12-fold increase in μ_h from P3HT nanogratings compared to thin films, indicating the positive effect of NIL on charge carrier transport in P3HT.[27] It is worth noting that they used large period gratings and observed that the mobility in the direction perpendicular to the gratings was higher than that parallel to them, which was contradictory to our results.[28] These different observations again indicate the potential geometric dependence of chain alignment and orientations. To further confirm this NIL-induced mobility increase in OPVs, it would be necessary to directly measure the vertical μ_h.

Nanoimprinted Electrode. In addition to active layer patterning to improve exciton dissociation and charge transport, NIL can also be used to pattern electrodes for OPVs in order to improve light transmission and charge collection. Nanoimprinted polymeric electrodes such as poly(3,4-ethylenedioxythiophene) (PEDOT) is of interest due to its high transparency, conductivity, and favorable work function. In the work from Pang *et al.*, to overcome the nonthermoplastic property of PEDOT, plasticizer glycerol was used to assist with nanoimprint at low temperature and pressure.[69,70] Guo *et al.* demonstrated a transfer imprint of PEDOT using a poly(dimethylsiloxane) (PDMS) mold followed by sequential inking and stamping steps.[71] The driving currents of the pentacene organic thin film transistors (OTFTs) with the patterned PEDOT contacts were greatly increased due to the high channel width-to-length ratio. This technique was also extended to the fabrication of a poly[2-methoxy-5-(2-ethylhexyloxy)-1,4-phenylene vinylene] (MEH-PPV) polymer light-emitting diode (PLED) using a roll-to-roll PEDOT imprint process. Nanoimprinted poly(3,4-ethylenedioxythiophene):poly(styrenesulfonate) (PEDOT:PSS), the water-soluble polymer mixture of PEDOT and PSS, is also of particular interest due to more convenient processing parameters for organic electronics. This work was first reported by Silva *et al.*[72] Their work demonstrated the feasibility of PEDOT:PSS patterning using NIL, and a 30% relative increase in PCE could be achieved in blended P3HT:PCBM solar cells with imprinted PEDOT:PSS nanogratings when compared to nonimprinted devices. It is worth noting that PEDOT:PSS nanogratings with extremely low aspect ratio (AR) ($\sim 10^{-2}$) were made and used in their work. To further increase the device performance, PEDOT:PSS nanostructures with a higher AR are desired. However, this goal is difficult to achieve due to the low cohesion of PEDOT:PSS molecules, which makes imprinted nanostructures easy to destroy during demolding.[73] To overcome this challenge, we developed a dehydration-assisted nanoimprint process to enhance the cohesion of PEDOT:PSS molecules and make high AR nanostructures.[31] The result of dehydration-assisted NIL is shown in Figure 5a. It can be seen that, after dehydration, high patterning fidelity and high-quality PEDOT:PSS nanostructures were possible due to the enhanced cohesion. Large-scale PEDOT:PSS nanogratings (2×2 cm^2) with height h = 60 nm, width w = 70 nm, and spacing p = 70 nm have been duplicated from a Si mold, resulting in an AR of 0.86 (h/w = 0.86).

Not only can the polymer electrode be patterned by NIL to improve solar cell performance, but many inorganic electrode materials can also be improved by this technique. Nanostructured metal oxide semiconductors for OPVs, such as ZnO and TiO_x processed using NIL, have been reported in literature.[74−78] As shown in Figure 5b, McGehee *et al.* fabricated TiO_2 nanostructures by NIL and found that P3HT:TiO_2 solar cells with patterned TiO_2 showed a 2-fold increase in J_{sc} and PCE over nonimprinted devices.[75] The improved efficiency was attributed to the enhanced charge separation and collection caused by increasing the interfacial area between TiO_2 and P3HT. Kang *et al.* showed that inexpensive metal materials could demonstrate similar performance as an anode when compared with ITO for organic solar cells.[30] In their work, they used NIL to fabricate metal-wire electrodes on Au, Cu, and Ag. Figure 5c shows the SEM image of a Cu wire electrode made using this technique. Similar optical transmission compared to conventional ITO electrodes was realized in the visible range while maintaining high electrical conductivity. With geometric optimization, blended P3HT:PCBM solar cells containing nanopatterned metal electrodes gave similar PCE to those with high-quality ITO electrodes. In their following work, they showed that a flexible transparent Cu nanowire mesh electrode could be fabricated by simple transfer printing from a PDMS mold, and an OPV using this flexible electrode gave comparable PCE to one using an ITO electrode.[79] Their work also demonstrated that the PCE of OPVs can be increased by 35% using a transparent plasmonic Ag

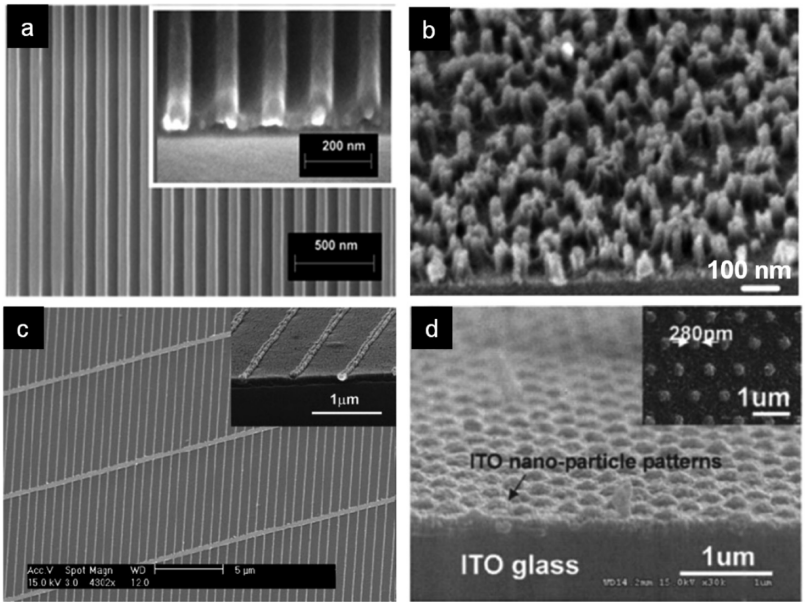

Figure 5. SEM images of various electrodes patterned by NIL: (a) PEDOT:PSS nanogratings; (b) TiO_2 nanorods; (c) Cu wire electrode; (d) directly patterned ITO nanoparticles on substrate. Image (a) reprinted with permission from ref 31. Copyright 2011 IOPscience. Image (b) reprinted from ref 75. Copyright 2008 American Chemical Society. Image (c) reprinted with permission from ref 30. Copyright 2008 John Wiley and Sons. Image (d) reprinted with permission from ref 82. Copyright 2009 American Institute of Physics.

nanowire electrode, despite the polarization dependence of the nanowire electrode and its lower transmittance than that of commercially available ITO-coated glass.[80] Very recently, they fabricated photonic color filters using periodic Au nanogratings. To harvest the light absorbed by these photonic color filters and avoid solar energy waste, P3HT:PCBM solar cells were built on these filters which also function as an anode. These dual-function devices might find applications in colored decorative OPVs.[81] In addition to this work on nanoimprinted metal electrodes, Lee *et al.* have demonstrated that the light transmission of indium tin oxide (ITO) could be increased by forming periodic ITO dot patterns on the ITO glass, as shown in Figure 5d.[82] In their work, a PDMS mold was used to pattern the ITO nanoparticle solution, directly forming periodic nanodots. ITO glass with the patterned ITO layer showed a 5% increase in transmission at 485 nm compared to that of ordinary ITO glass.

Challenges and Future Tasks. To date, much progress has been achieved in nanoimprinted polymer solar cells. However, there are still many challenges existing in this field. To further widen the application of NIL in OPVs, three important factors, including the process window, cost and throughput, and efficiency, need to be considered.

Process Window for New Materials. The first challenge comes from the unknown process window, that is, the question of whether NIL can be applied to new conjugated materials which give higher efficiency than P3HT. To date, most work on nanoimprinted OPVs has been focused on P3HT, due to its convenience for nanoimprint patterning, high PCE when combined with PCBM in BHJ architecture (4−5%), and commercial availability.[59,60] However, many groups have reported much higher efficiencies by using new conjugated polymers. For example, Heeger *et al.* showed that an efficiency up to 6.1% could be obtained by using poly[*N*′′-900-heptadecanyl-2,7-carbazole-*alt*-5,5-(4′,7′-di-2-thienyl-2′,1′,3′-benzothiadiazole)] (PCDTBT) in bulk heterojunction composites with the fullerene derivative [6,6]-phenyl-C_{70}-butyric acid methyl ester ($PC_{70}BM$).[6] Later, 7.4% PCE was announced by Yu *et al.* using a bulk heterojunction composed of a polymer of thieno[3,4-*b*]thiophene and benzodithiophene (PTB) family PTB7 and $PC_{71}BM$.[7] So far, no work has been reported showing the effect of NIL on these champion polymers. If NIL is to become a useful technique for the organic solar cell industry in the future, the feasibility of using NIL to improve the device performance of these new polymers needs to be addressed.

Cost and Throughput. For any nanofabrication process, maintaining both low-cost and high-throughput is always desired.[83] Therefore, it is critical for nanoimprinted OPVs to simplify fabrication, lower costs, and increase throughput. Although many people have demonstrated that the PCE of polymer solar cells can be improved by NIL, the required fabrication procedures are more complicated and thus more costly than the most common blended BHJ solar cells. For example, e-beam lithography is the most widely used technique to fabricate molds with nanoscale sizes,[84] but due to the complicated and long fabrication procedures, it is extremely expensive to make molds with large feature areas. Fabrication of molds with

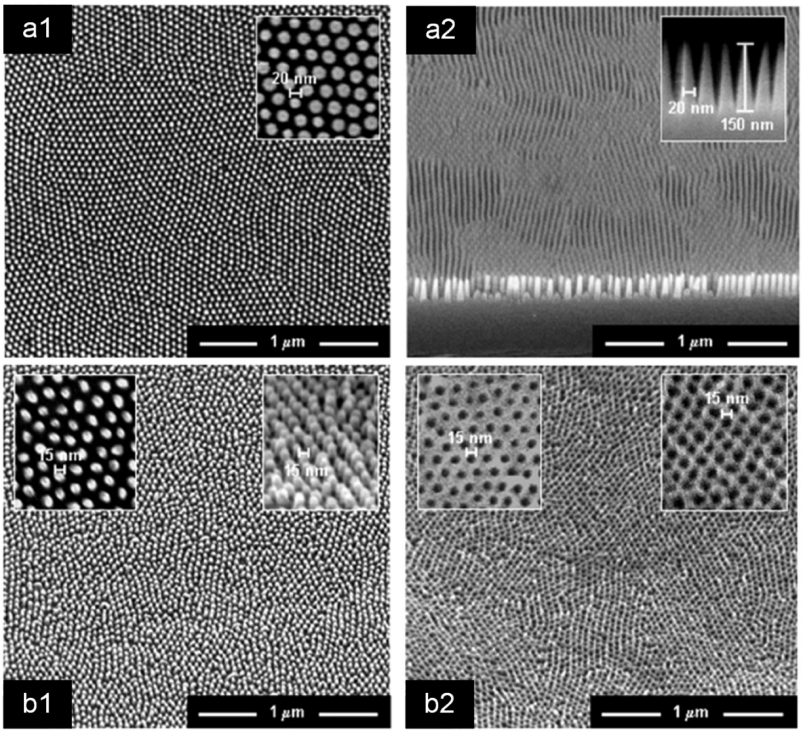

Figure 6. SEM images of (a) SiO_2 molds fabricated by the transfer of the block copolymer PS-*b*-PMMA nanopatterns onto the SiO_2 layer: (a1) nanohole and (a2) nanopillar molds with 20 nm diameter. (b) Imprinted P3HT nanostructures: (b1) nanopillar and (b2) nanohole structures with 15 nm diameter. Images reprinted from ref 86. Copyright 2009 American Chemical Society.

small feature sizes and large area, while keeping a low cost, will need to rely on other simpler techniques; much progress in this area has been reported.[34,41,49,85−87] For example, we have developed a robust but low-cost method to make Si molds over 4 in. by inductively coupled plasma etching using freestanding anodic alumina membranes (AAMs) as an etch mask.[34] Another example is large-area, high AR, sub-20 nm SiO_2 nanopillar and nanohole molds made by Guo *et al.*, as shown in Figure 6a,b.[86] In their work, SiO_2 molds were fabricated through the transfer of nanopatterns of the block copolymer poly(styrene)-*block*-poly(methyl methacrylate) (PS-*b*-PMMA) onto an SiO_2 layer. P3HT nanopillars and nanoholes with 15 nm diameters were realized using these molds; this size is, to the best of the authors' knowledge, the smallest ever reported. Their work has demonstrated the possibility of achieving the ideal OPV structure, that is, precise phase separation at the scale of exciton diffusion length (~10 nm). Besides the fabrication of molds at lower cost, nanoimprint at lower temperatures and pressures is also desired. Much progress on low temperature and pressure NIL has been reported from different groups.[88−93] For conjugated polymer patterning at low temperature, the solvent-assisted nanoimprint of polymer solar cells demonstrated by different groups has been shown to be a promising approach.[38,39,90]

Another important and effective way to increase the throughput of nanoimprinted solar cells comes from the roll-to-roll (R2R) imprint process instead of the conventional planar nanoimprint scheme. This continuous process has been studied and exhibited by several groups.[94−97] For example, as shown in Figure 7(a-d), Ahn et al. have demonstrated their work on R2R and roll-to-plate (R2P) NIL.[94] In their work, large-area (4 in. wide) imprinted epoxysilicone nanogratings with 300 nm line width grating structures on both hard substrate glass and flexible substrate PET have been realized by developing a apparatus capable of both R2R and R2P NIL processes. Polymer solar cells made by roller printing have also been realized by different groups.[98−102] However, to date, no one has reported nanoimprinted polymer solar cells made using this roll-to-roll method. Multidisciplinary collaborations are required to realize this high-throughput fabrication.

Efficiency. The third challenge is how to further improve the performance of nanoimprinted polymer solar cells. In literature, people have shown that devices made by this technique give higher efficiencies than bilayer structures, but the highest efficiencies using the same donor and acceptor materials are still lower than the best reported performance using the BHJ structure. One important reason could be that the sizes of imprinted nanostructures in literature are still larger than the exciton diffusion length, and the thicknesses are shorter than the photon mean free path. However, technically fabricating a polymer nanostructure with high aspect ratio and small width can be challenging. For example, as shown in Figure 8a, Tao *et al.* demonstrated that, during demolding, the

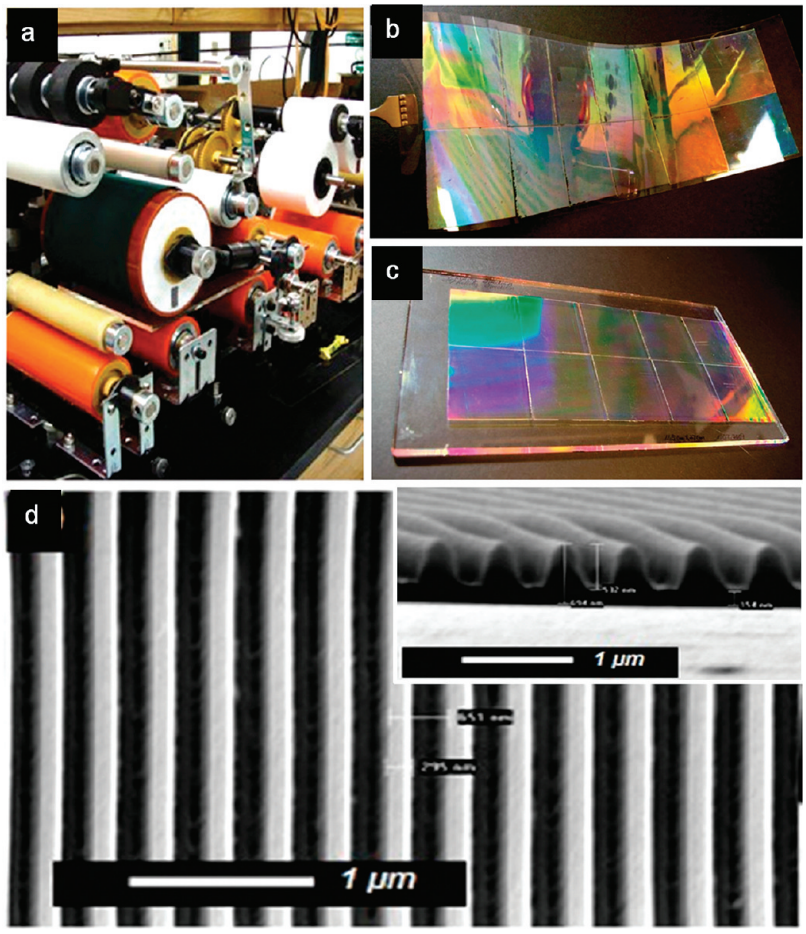

Figure 7. Photograph of (a) R2R/R2P NIL apparatus, (b) 4 in. wide and 12 in. long 700 nm period epoxysilicone pattern on flexible PET substrate by R2R NIL process, and (c) 4 in. wide and 10.5 in. long 700 nm period grating pattern on glass substrate. (d) SEM images of the patterned grating structure. Images reprinted from ref 94. Copyright 2009 American Chemical Society.

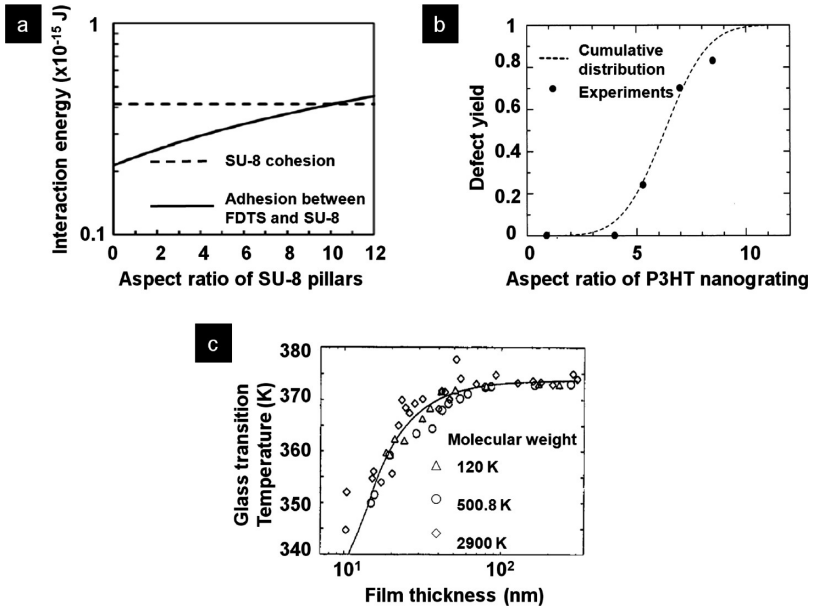

Figure 8. Summary of polymer geometric effects: (a) cohesion energy of SU-8 pillars and their adhesion with the mold as a function of the aspect ratio of the nanopillars; (b) relation between defect yield of transfer imprinted P3HT nanostructures and their aspect ratios; (c) T_g as a function of film thickness for polystyrene. Images reprinted with permission from the references as indicated: (a) ref 103. Copyright 2010 IOPscience; (b) ref 104. Copyright 2011 Japan Science and Technology Information Aggregator, Electronic; (c) ref 105. Copyright 1994 EDP Sciences.

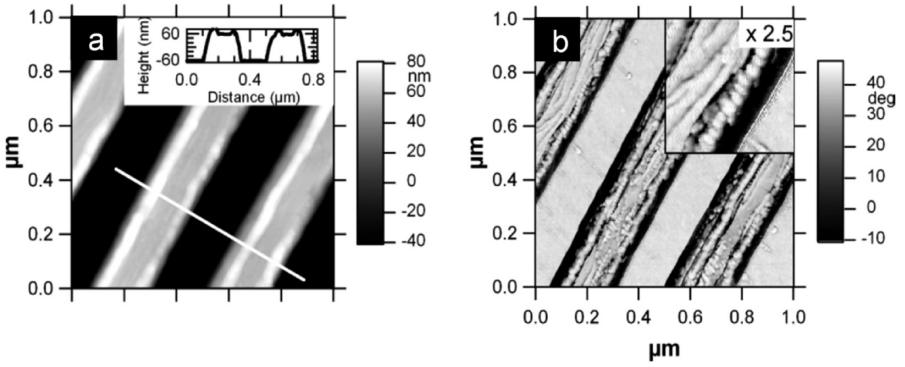

Figure 9. Nonuniform distribution of NIL-induced chain alignment in PVDF: AFM (a) height and (b) phase images of PVDF film crystallized by nanoimprint, showing the presence of excess material at the wall of the trench and the increased crystals at the trench walls. Images reprinted from ref 66. Copyright 2005 American Chemical Society.

imprinted polymer nanostructure, such as SU-8, could be destroyed more readily as the aspect ratio increases, making the adhesion between mold and polymer higher than the polymer cohesion.[103] By studying the relationship between the defect yield of transfer imprinted P3HT nanogratings and their aspect ratios, Hirai *et al.* found that the AR needed to be limited to below 3 if complete P3HT nanogratings were desired, and that nanostructures were narrowly transferred when the aspect ratio went to 8.5, as shown in Figure 8b.[104] In addition to the challenge of achieving high aspect ratios, it may also be difficult to maintain good mechanical strength when the imprinted conjugated polymer nanostructure's size decreases close to the exciton diffusion lengths (*i.e.*, below 10 nm). Keddie *et al.* have shown that the T_g for polymers such as polystyrene could drop greatly, from 375 to 340 K, when its thickness decreased to ~10 nm, as shown in Figure 8c.[105] Besides these technical limitations, note that the optimal height of imprinted polymer nanostructures is determined by light interference and charge mobility, as well.[106] As demonstrated in literature, the chain alignment in imprinted conjugated polymers can improve hole mobility, which allows for a higher nanostructure. However, it is noted that there is a size limit for NIL-induced chain alignment in conjugated polymers. For example, Hu *et al.* have found that the NIL-induced chain alignment in PVDF was nonuniform and more present close to the mold trench walls,[66] as shown in Figure 9a,b. Taking into account these findings, it is reasonable to conclude that there must be a practical maximum IEF and minimum nanostructure width for each conjugated polymer used for OPVs. Further studies are required with respect to these factors.

Like bilayer polymer solar cells, nanoimprinted polymer solar cells are typically made through the deposition of one material onto the second, making these two layers' electrical properties relatively independent. It is thus reasonable to speculate that the challenges occurring at the donor/acceptor interface in bilayer structures exist in imprinted devices, as well. For example, a critical factor limiting the PCE of bilayer polymer solar cells is the mismatch between hole and electron mobilities. In BHJ structures, the charge carrier mobilities are more balanced due to the interaction between polymer and fullerenes.[60,107] However, in bilayer solar cells, where μ_h is typically 2 to 3 orders of magnitude lower than electron mobility (μ_e), the hole accumulation at the anode results in space−charge limited current.[108] The photocurrent has a square-root dependence on bias, and thus a FF above 40% is difficult to achieve.[109] If μ_h and μ_e could be balanced, as demonstrated by Schwartz *et al.* in their bilayer P3HT/PCBM solar cells, FF and PCE up to 63 and 3.5%, respectively, could be achieved. This strongly demonstrates the effects of mobility balance on device performance.[40] One approach to balance the charge mobility for nanoimprinted OPVs is NIL-induced chain alignment as discussed previously. Zhou *et al.* have shown that the field effect μ_h in P3HT nanogratings could be increased to $\sim 3 \times 10^{-2}$ $cm^2 \cdot V^{-1} \cdot s^{-1}$, which is comparable to μ_e reported in literature.[28]

Besides the issue of mobility mismatch, the donor/acceptor interface of nanoimprinted polymer solar cells need to be studied carefully, as well. Theoretically, a sharp interface between the donor and acceptor is needed for efficient charge separation. However, people have found that there are a large number of grain boundaries, defects, and interface trap states at the pristine polymer and fullerene bilayer interface, which decrease the device performance.[110] In bilayer devices, postannealing can be applied to solve this problem, by causing the diffusion of the two materials into one another, forming a more intimate donor/acceptor interface.[110−114] When applied to nanoimprinted solar cells, one concern might be that the imprinted nanostructures can melt at high annealing temperature and decrease performance. However, it has been shown that postannealing did improve the PCE of nanoimprinted solar cells, similarly to the bilayer structure, even after high temperature treatment.[28,37] A possible

answer to this phenomenon might be that, in these studies, the widths of imprinted nanostructures were larger than the exciton diffusion length. Postannealing made the imprinted polymer nanostructure and fullerene diffuse into one another, forming even better phase separation at scales closer to the exciton diffusion length. Hlaing *et al.* have shown that the NIL-induced P3HT chain alignment could be maintained when the imprinted nanostructures were melted at a high annealing temperature.[33] These findings prove that postannealing can be an effective way to improve the interface of imprinted polymer/fullerene solar cells without any changes in chain orientation. Despite these findings, it is worth noting that annealing can have an opposite effect, that is, decrease the PCE of bilayer polymer solar cells in some cases, depending on each material's specific properties. For example, McNeill *et al.* have proven that annealing decreased the performance of polyfluorene copolymers poly(9,9-dioctylfluorene-*co*-bis(*N*,*N*′-(4,butylphenyl))bis(*N*,*N*′-phenyl-1,4-phenylene)diamine) (PFB) and F8BT solar cells because it decreased the hole and electron mobilities and increased disorder at the PFB/F8BT interface, resulting in low exciton dissociation.[115] These findings suggest that alternative ways need to be developed to improve the donor/acceptor interface when annealing does not apply, and each material combination should be carefully studied.

CONCLUSIONS

Recent progress from nanoimprinted polymer solar cells has made NIL a new and promising technique by which the active layer morphology can be greatly controlled and optimized. Simultaneous control of both efficient exciton dissociation and charge transport, which are regarded as two important factors limiting the performance of organic solar cells, becomes realistic using this technique. Various fabrication methods have been developed to make nanoimprinted polymer solar cells. One approach to further improve the efficiency of nanoimprinted solar cells is to optimize the geometry of nanostructures formed by NIL to maximize the exciton dissociation rate; the feasibility of this method has been proven by several studies from different groups. In addition, it has been found that a more favorable chain alignment, which can assist hole transport in conjugated polymers, can be realized when polymer thin films are patterned using a hydrophobic Si mold. Some preliminary studies have observed that hole mobility can be enhanced in nanoimprinted P3HT. NIL-introduced electrode patterning also provides an alternative approach to improve the PCE of polymer solar cells. To integrate NIL into the future OPV industry, advancements in nanoimprinted OPVs need to include testing the process window of NIL on different conjugated polymers, increasing the throughput of this technique at low cost and further improving the PCE of this type of solar cell.

Conflict of Interest: The authors declare no competing financial interest.

Acknowledgment. This work is supported by National Science Foundation (No. ECCS-0901759), Welch Foundation Grant AT-1617, and DOE Phase II STTR program on "Hybrid Tandem Solar Cells", Grant No. DE-SC00003664. The authors gratefully acknowledge J. Hsu from Department of Materials Science and Engineering at UT Dallas for her support and helpful discussions.

REFERENCES AND NOTES

1. Lewis, N. S. Toward Cost-Effective Solar Energy Use. *Science* **2007**, *315*, 798–801.
2. Service, R. F. Outlook Brightens for Plastic Solar Cells. *Science* **2011**, *332*, 293.
3. Spanggaard, H.; Krebs, F. C. A Brief History of the Development of Organic and Polymeric Photovoltaics. *Sol. Energy Mater. Sol. Cells* **2004**, *83*, 125–146.
4. Sariciftci, N. S.; Smilowitz, L.; Heeger, A. J.; Wudl, F. Photoinduced Electron-Transfer from a Conducting Polymer to Buckminsterfullerene. *Science* **1992**, *258*, 1474–1476.
5. Brabec, C. J.; Sariciftci, N. S.; Hummelen, J. C. Plastic Solar Cells. *Adv. Funct. Mater.* **2001**, *11*, 15–26.
6. Park, S. H.; Roy, A.; Beaupre, S.; Cho, S.; Coates, N.; Moon, J. S.; Moses, D.; Leclerc, M.; Lee, K.; Heeger, A. J. Bulk Heterojunction Solar Cells with Internal Quantum Efficiency Approaching 100%. *Nat. Photonics* **2009**, *3*, 297–302.
7. Liang, Y.; Xu, Z.; Xia, J.; Tsai, S.-T.; Wu, Y.; Li, G.; Ray, C.; Yu, L. For the Bright Future-Bulk Heterojunction Polymer Solar Cells with Power Conversion Efficiency of 7.4%. *Adv. Mater.* **2010**, *22*, E135–E138.
8. Brabec, C. J.; Hauch, J. A.; Schilinsky, P.; Waldauf, C. Production Aspects of Organic Photovoltaics and Their Impact on the Commercialization of Devices. *MRS Bull.* **2005**, *30*, 50–52.
9. Kroeze, J. E.; Savenije, T. J.; Vermeulen, M. J. W.; Warman, J. M. Contactless Determination of the Photoconductivity Action Spectrum, Exciton Diffusion Length, and Charge Separation Efficiency in Polythiophene-Sensitized TiO_2 Bilayers. *J. Phys. Chem. B* **2003**, *107*, 7696–7705.
10. Peumans, P.; Yakimov, A.; Forrest, S. R. Small Molecular Weight Organic Thin-Film Photodetectors and Solar Cells. *J. Appl. Phys.* **2003**, *93*, 3693–3723.
11. Haugeneder, A.; Neges, M.; Kallinger, C.; Spirkl, W.; Lemmer, U.; Feldmann, J.; Scherf, U.; Harth, E.; Gugel, A.; Mullen, K. Exciton Diffusion and Dissociation in Conjugated Polymer Fullerene Blends and Heterostructures. *Phys. Rev. B* **1999**, *59*, 15346–15351.
12. Stubinger, T.; Brutting, W. Exciton Diffusion and Optical Interference in Organic Donor–Acceptor Photovoltaic Cells. *J. Appl. Phys.* **2001**, *90*, 3632–3641.
13. Blom, P. W. M.; deJong, M. J. M.; vanMunster, M. G. Electric-Field and Temperature Dependence of the Hole Mobility in Poly(*p*-phenylene vinylene). *Phys. Rev. B* **1997**, *55*, R656–R659.
14. Li, G.; Shrotriya, V.; Yao, Y.; Yang, Y. Investigation of Annealing Effects and Film Thickness Dependence of Polymer Solar Cells Based on Poly(3-hexylthiophene). *J. Appl. Phys.* **2005**, *98*, 043704.
15. Halls, J. J. M.; Walsh, C. A.; Greenham, N. C.; Marseglia, E. A.; Friend, R. H.; Moratti, S. C.; Holmes, A. B. Efficient Photodiodes from Interpenetrating Polymer Networks. *Nature* **1995**, *376*, 498–500.
16. Yu, G.; Gao, J.; Hummelen, J. C.; Wudl, F.; Heeger, A. J. Polymer Photovoltaic Cells - Enhanced Efficiencies *via* a Network of Internal Donor–Acceptor Heterojunctions. *Science* **1995**, *270*, 1789–1791.

17. Hoppe, H.; Niggemann, M.; Winder, C.; Kraut, J.; Hiesgen, R.; Hinsch, A.; Meissner, D.; Sariciftci, N. S. Nanoscale Morphology of Conjugated Polymer/Fullerene-Based Bulk-Heterojunction Solar Cells. *Adv. Funct. Mater.* **2004**, *14*, 1005–1011.
18. Watkins, P. K.; Walker, A. B.; Verschoor, G. L. B. Dynamical Monte Carlo Modelling of Organic Solar Cells: The Dependence of Internal Quantum Efficiency on Morphology. *Nano Lett.* **2005**, *5*, 1814–1818.
19. Slota, J. E.; He, X.; Huck, W. T. S. Controlling Nanoscale Morphology in Polymer Photovoltaic Devices. *Nano Today* **2010**, *5*, 231–242.
20. Yang, F.; Forrest, S. R. Photocurrent Generation in Nanostructured Organic Solar Cells. *ACS Nano* **2008**, *2*, 1022–1032.
21. Chen, J.-T.; Hsu, C.-S. Conjugated Polymer Nanostructures for Organic Solar Cell Applications. *Polym. Chem.* **2011**, *2*, 2707–2722.
22. Weickert, J.; Dunbar, R. B.; Hesse, H. C.; Wiedemann, W.; Schmidt-Mende, L. Nanostructured Organic and Hybrid Solar Cells. *Adv. Mater.* **2011**, *23*, 1810–1828.
23. Chou, S. Y.; Krauss, P. R.; Renstrom, P. J. Imprint Lithography with 25-Nanometer Resolution. *Science* **1996**, *272*, 85–87.
24. Chou, S. Y.; Krauss, P. R.; Zhang, W.; Guo, L. J.; Zhuang, L. Sub-10 nm Imprint Lithography and Applications. *J. Vac. Sci. Technol., B* **1997**, *15*, 2897–2904.
25. Guo, L. J. Recent Progress in Nanoimprint Technology and Its Applications. *J. Phys. D: Appl. Phys.* **2004**, *37*, R123–R141.
26. Zheng, Z.; Yim, K.-H.; Saifullah, M. S. M.; Welland, M. E.; Friend, R. H.; Kim, J.-S.; Huck, W. T. S. Uniaxial Alignment of Liquid-Crystalline Conjugated Polymers by Nanoconfinement. *Nano Lett.* **2007**, *7*, 987–992.
27. Cui, D.; Li, H.; Park, H.; Cheng, X. Improving Organic Thin-Film Transistor Performance by Nanoimprint-Induced Chain Ordering. *J. Vac. Sci. Technol., B* **2008**, *26*, 2404–2409.
28. Zhou, M.; Aryal, M.; Mielczarek, K.; Zakhidov, A.; Hu, W. Hole Mobility Enhancement by Chain Alignment in Nanoimprinted Poly(3-hexylthiophene) Nanogratings for Organic Electronics. *J. Vac. Sci. Technol., B* **2010**, *28*, C6M63–C6M67.
29. Ko, D.-H.; Tumbleston, J. R.; Gadisa, A.; Aryal, M.; Liu, Y.; Lopez, R.; Samulski, E. T. Light-Trapping Nano-Structures in Organic Photovoltaic Cells. *J. Mater. Chem.* **2011**, *21*, 16293–16303.
30. Kang, M.-G.; Kim, M.-S.; Kim, J.; Guo, L. J. Organic Solar Cells Using Nanoimprinted Transparent Metal Electrodes. *Adv. Mater.* **2008**, *20*, 4624–4624.
31. Yang, Y.; Lee, K.; Mielczarek, K.; Hu, W.; Zakhidov, A. Nanoimprint of Dehydrated PEDOT:PSS for Organic Photovoltaics. *Nanotechnology* **2011**, *22*, 485301.
32. Aryal, M.; Trivedi, K.; Hu, W. Nano-Confinement Induced Chain Alignment in Ordered P3HT Nanostructures Defined by Nanoimprint Lithography. *ACS Nano* **2009**, *3*, 3085–3090.
33. Hlaing, H.; Lu, X.; Hofmann, T.; Yager, K. G.; Black, C. T.; Ocko, B. M. Nanoimprint-Induced Molecular Orientation in Semiconducting Polymer Nanostructures. *ACS Nano* **2011**, *5*, 7532–7538.
34. Aryal, M.; Buyukserin, F.; Mielczarek, K.; Zhao, X.; Gao, J.; Zakhidov, A.; Hu, W. Imprinted Large-Scale High Density Polymer Nanopillars for Organic Solar Cells. *J. Vac. Sci. Technol., B* **2008**, *26*, 2562–2566.
35. Wiedemann, W.; Sims, L.; Abdellah, A.; Exner, A.; Meier, R.; Musselman, K. P.; MacManus-Driscoll, J. L.; Mueller-Buschbaum, P.; Scarpa, G.; Lugli, P.; Schmidt-Mende, L. Nanostructured Interfaces in Polymer Solar Cells. *Appl. Phys. Lett.* **2010**, *96*, 263109.
36. Cheyns, D.; Vasseur, K.; Rolin, C.; Genoe, J.; Poortmans, J.; Heremans, P. Nanoimprinted Semiconducting Polymer Films with 50 nm Features and Their Application to Organic Heterojunction Solar Cells. *Nanotechnology* **2008**, *19*, 424016.
37. Yang, Y.; Aryal, M.; Mielczarek, K.; Hu, W.; Zakhidov, A. Nanoimprinted P3HT/C_{60} Solar Cells Optimized by Oblique Deposition of C_{60}. *J. Vac. Sci. Technol., B* **2010**, *28*, C6M104–C6M107.
38. He, X.; Gao, F.; Tu, G.; Hasko, D.; Huettner, S.; Steiner, U.; Greenham, N. C.; Friend, R. H.; Huck, W. T. S. Formation of Nanopatterned Polymer Blends in Photovoltaic Devices. *Nano Lett.* **2010**, *10*, 1302–1307.
39. He, X.; Gao, F.; Tu, G.; Hasko, D. G.; Huettner, S.; Greenham, N. C.; Steiner, U.; Friend, R. H.; Huck, W. T. S. Formation of Well-Ordered Heterojunctions in Polymer: PCBM Photovoltaic Devices. *Adv. Funct. Mater.* **2011**, *21*, 139–146.
40. Ayzner, A. L.; Tassone, C. J.; Tolbert, S. H.; Schwartz, B. J. Reappraising the Need for Bulk Heterojunctions in Polymer-Fullerene Photovoltaics: The Role of Carrier Transport in All-Solution-Processed P3HT/PCBM Bilayer Solar Cells. *J. Phys. Chem. C* **2009**, *113*, 20050–20060.
41. Avnon, E.; Yaacobi-Gross, N.; Ploshnik, E.; Shenhar, R.; Tessler, N. Low Cost, Nanometer Scale Nanoimprinting - Application to Organic Solar Cells Optimization. *Org. Electron.* **2011**, *12*, 1241–1246.
42. Zeng, W.; Chong, K. S. L.; Low, H. Y.; Williams, E. L.; Tam, T. L.; Sellinger, A. The Use of Nanoimprint Lithography To Improve Efficiencies of Bilayer Organic Solar Cells Based on P3HT and a Small Molecule Acceptor. *Thin Solid Films* **2009**, *517*, 6833–6836.
43. Karabacak, T.; Lu, T. M. Enhanced Step Coverage by Oblique Angle Physical Vapor Deposition. *J. Appl. Phys.* **2005**, *97*, 124504.
44. Cocoyer, C.; Rocha, L.; Sicot, L.; Geffroy, B.; de Bettignies, R.; Sentein, C.; Fiorini-Debuisschert, C.; Raimond, P. Implementation of Submicrometric Periodic Surface Structures toward Improvement of Organic-Solar-Cell Performances. *Appl. Phys. Lett.* **2006**, *88*, 2188600.
45. Matterson, B. J.; Lupton, J. M.; Safonov, A. F.; Salt, M. G.; Barnes, W. L.; Samuel, I. D. W. Increased Efficiency and Controlled Light Output from a Microstructured Light-Emitting Diode. *Adv. Mater.* **2001**, *13*, 123–127.
46. Rang, Z. L.; Nathan, M. I.; Ruden, P. P.; Chesterfield, R.; Frisbie, C. D. Hydrostatic-Pressure Dependence of Organic Thin-Film Transistor Current *versus* Voltage Characteristics. *Appl. Phys. Lett.* **2004**, *85*, 5760–5762.
47. Schroepfer, D. D.; Ruden, P. P.; Xia, Y.; Frisbie, C. D.; Shaheen, S. E. Hydrostatic Pressure Effects on Poly(3-hexylthiophene) Thin Film Transistors. *Appl. Phys. Lett.* **2008**, *92*, 013305.
48. Shih, C. F.; Hung, K. T.; Wu, J. W.; Hsiao, C. Y.; Li, W. M. Efficiency Improvement of Blended Poly(3-hexylthiophene) and 1-(3-Methoxycarbonyl)-propyl-1-phenyl-(6,6)C_{61} Solar Cells by Nanoimprinting. *Appl. Phys. Lett.* **2009**, *94*, 143505.
49. Lee, J. H.; Kim, D. W.; Jang, H.; Choi, J. K.; Geng, J.; Lung, J. W.; Yoon, S. C.; Jung, H.-T. Enhanced Solar-Cell Efficiency in Bulk-Heterojunction Polymer Systems Obtained by Nanoimprinting with Commercially Available AAO Membrane Fitters. *Small* **2009**, *5*, 2139–2143.
50. Wiedenmann, O.; Abdellah, A.; Scarpa, G.; Lugli, P. Design and Fabrication of Organic Solar Cells Structured *via* Nanoimprint Lithography. *J. Phys.: Conf. Ser.* **2009**, *193*, 012115.
51. Kim, J.; Kim, K.; Hwan, Ko, S.; Kim, W. Optimum Design of Ordered Bulk Heterojunction Organic Photovoltaics. *Sol. Energy Mater. Sol. Cells* **2011**, *95*, 3021–3024.
52. Kim, M.-S.; Kim, J.-S.; Cho, J. C.; Shtein, M.; Guo, L. J.; Kim, J. Flexible Conjugated Polymer Photovoltaic Cells with Controlled Heterojunctions Fabricated Using Nanoimprint Lithography. *Appl. Phys. Lett.* **2007**, *90*, 123113.
53. Sirringhaus, H.; Brown, P. J.; Friend, R. H.; Nielsen, M. M.; Bechgaard, K.; Langeveld-Voss, B. M. W.; Spiering, A. J. H.; Janssen, R. A. J.; Meijer, E. W.; Herwig, P.; de Leeuw, D. M. Two-Dimensional Charge Transport in Self-Organized, High-Mobility Conjugated Polymers. *Nature* **1999**, *401*, 685–688.
54. Chen, T. A.; Wu, X. M.; Rieke, R. D. Regiocontrolled Synthesis of Poly(3-alkylthiophenes) Mediated by Rieke Zinc - Their Characterization and Solid-State Properties. *J. Am. Chem. Soc.* **1995**, *117*, 233–244.

55. Zhokhavets, U.; Erb, T.; Hoppe, H.; Gobsch, G.; Sariciftci, N. S. Effect of Annealing of Poly(3-hexylthiophene)/Fullerene Bulk Heterojunction Composites on Structural and Optical Properties. *Thin Solid Films* **2006**, *496*, 679–682.
56. Erb, T.; Zhokhavets, U.; Gobsch, G.; Raleva, S.; Stuhn, B.; Schilinsky, P.; Waldauf, C.; Brabec, C. J. Correlation between Structural and Optical Properties of Composite Polymer/Fullerene Films for Organic Solar Cells. *Adv. Funct. Mater.* **2005**, *15*, 1193–1196.
57. Sirringhaus, H.; Wilson, R. J.; Friend, R. H.; Inbasekaran, M.; Wu, W.; Woo, E. P.; Grell, M.; Bradley, D. D. C. Mobility Enhancement in Conjugated Polymer Field-Effect Transistors through Chain Alignment in a Liquid-Crystalline Phase. *Appl. Phys. Lett.* **2000**, *77*, 406–408.
58. Kim, Y.; Choulis, S. A.; Nelson, J.; Bradley, D. D. C.; Cook, S.; Durrant, J. R. Device Annealing Effect in Organic Solar Cells with Blends of Regioregular Poly(3-hexylthiophene) and Soluble Fullerene. *Appl. Phys. Lett.* **2005**, *86*, 063502.
59. Ma, W. L.; Yang, C. Y.; Gong, X.; Lee, K.; Heeger, A. J. Thermally Stable, Efficient Polymer Solar Cells with Nanoscale Control of the Interpenetrating Network Morphology. *Adv. Funct. Mater.* **2005**, *15*, 1617–1622.
60. Li, G.; Shrotriya, V.; Huang, J. S.; Yao, Y.; Moriarty, T.; Emery, K.; Yang, Y. High-Efficiency Solution Processable Polymer Photovoltaic Cells by Self-Organization of Polymer Blends. *Nat. Mater.* **2005**, *4*, 864–868.
61. Brinkmann, M.; Wittmann, J. C. Orientation of Regioregular Poly(3-hexylthiophene) by Directional Solidification: A Simple Method To Reveal the Semicrystalline Structure of a Conjugated Polymer. *Adv. Mater.* **2006**, *18*, 860–863.
62. Kline, R. J.; McGehee, M. D.; Toney, M. F. Highly Oriented Crystals at the Buried Interface in Polythiophene Thin-Film Transistors. *Nat. Mater.* **2006**, *5*, 222–228.
63. Hu, Z.; Jonas, A. M. Control of Crystal Orientation in Soft Nanostructures by Nanoimprint Lithography. *Soft Matter* **2010**, *6*, 21–28.
64. Schmid, S. A.; Yim, K. H.; Chang, M. H.; Zheng, Z.; Huck, W. T. S.; Friend, R. H.; Kim, J. S.; Herz, L. M. Polarization Anisotropy Dynamics for Thin Films of a Conjugated Polymer Aligned by Nanoimprinting. *Phys. Rev. B* **2008**, *77*, 115338.
65. Rowland, H. D.; King, W. P.; Pethica, J. B.; Cross, G. L. W. Molecular Confinement Accelerates Deformation of Entangled Polymers during Squeeze Flow. *Science* **2008**, *322*, 720–724.
66. Hu, Z. J.; Baralia, G.; Bayot, V.; Gohy, J. F.; Jonas, A. M. Nanoscale Control of Polymer Crystallization by Nanoimprint Lithography. *Nano Lett.* **2005**, *5*, 1738–1743.
67. Coakley, K. M.; Srinivasan, B. S.; Ziebarth, J. M.; Goh, C.; Liu, Y. X.; McGehee, M. D. Enhanced Hole Mobility in Regioregular Polythiophene Infiltrated in Straight Nanopores. *Adv. Funct. Mater.* **2005**, *15*, 1927–1932.
68. Al-Assaad, R. M.; Regonda, S.; Tao, L.; Pang, S. W.; Hu, W. W. Characterizing Nanoimprint Profile Shape and Polymer Flow Behavior Using Visible Light Angular Scatterometry. *J. Vac. Sci. Technol., B* **2007**, *25*, 2396–2401.
69. Reano, R. M.; Kong, Y. P.; Low, H. Y.; Tan, L.; Wang, F.; Pang, S. W.; Yee, A. F. Stability of Functional Polymers after Plasticizer-Assisted Imprint Lithography. *J. Vac. Sci. Technol., B* **2004**, *22*, 3294–3299.
70. Tan, L.; Kong, Y. P.; Pang, S. W.; Yee, A. F. Imprinting of Polymer at Low Temperature and Pressure. *J. Vac. Sci. Technol., B* **2004**, *22*, 2486–2492.
71. Li, D.; Guo, L. J. Organic Thin Film Transistors and Polymer Light-Emitting Diodes Patterned by Polymer Inking and Stamping. *J. Phys. D: Appl. Phys.* **2008**, *41*, 105115.
72. Emah, J. B.; Curry, R. J.; Silva, S. R. P. Low Cost Patterning of Poly(3,4-ethylenedioxythiophene) Poly(styrenesulfonate) Films To Increase Organic Photovoltaic Device Efficiency. *Appl. Phys. Lett.* **2008**, *93*, 103301.
73. Lang, U.; Naujoks, N.; Dual, J. Mechanical Characterization of PEDOT:PSS Thin Films. *Synth. Met.* **2009**, *159*, 473–479.
74. Yang, K.-Y.; Yoon, K.-M.; Choi, K.-W.; Lee, H. The Direct Nano-Patterning of ZnO Using Nanoimprint Lithography with ZnO-Sol and Thermal Annealing. *Microelectron. Eng.* **2009**, *86*, 2228–2231.
75. Williams, S. S.; Hampton, M. J.; Gowrishankar, V.; Ding, I. K.; Templeton, J. L.; Samulski, E. T.; DeSimone, J. M.; McGehee, M. D. Nanostructured Titania-Polymer Photovoltaic Devices Made Using PFPE-Based Nanomolding Techniques. *Chem. Mater.* **2008**, *20*, 5229–5234.
76. Baek, W.-H.; Seo, I.; Yoon, T.-S.; Lee, H. H.; Yun, C. M.; Kim, Y.-S. Hybrid Inverted Bulk Heterojunction Solar Cells with Nanoimprinted TiO_2 Nanopores. *Sol. Energy Mater. Sol. Cells* **2009**, *93*, 1587–1591.
77. Treat, N. D.; Campos, L. M.; Dimitriou, M. D.; Ma, B.; Chabinyc, M. L.; Hawker, C. J. Nanostructured Hybrid Solar Cells: Dependence of the Open Circuit Voltage on the Interfacial Composition. *Adv. Mater.* **2010**, *22*, 4982–4986.
78. Her, H.-J.; Kim, J.-M.; Kang, C. J.; Kim, Y.-S. Hybrid Photovoltaic Cell with Well-Ordered Nanoporous Titania-P3HT by Nanoimprinting Lithography. *J. Phys. Chem. Solids* **2008**, *69*, 1301–1304.
79. Kang, M.-G.; Park, H. J.; Ahn, S. H.; Guo, L. J. Transparent Cu Nanowire Mesh Electrode on Flexible Substrates Fabricated by Transfer Printing and Its Application in Organic Solar Cells. *Sol. Energy Mater. Sol. Cells* **2010**, *94*, 1179–1184.
80. Kang, M.-G.; Xu, T.; Park, H. J.; Luo, X.; Guo, L. J. Efficiency Enhancement of Organic Solar Cells Using Transparent Plasmonic Ag Nanowire Electrodes. *Adv. Mater.* **2010**, *22*, 4378–4383.
81. Park, H. J.; Xu, T.; Lee, J. Y.; Ledbetter, A.; Guo, L. J. Photonic Color Filters Integrated with Organic Solar Cells for Energy Harvesting. *ACS Nano* **2011**, *5*, 7055–7060.
82. Yang, K.-Y.; Yoon, K.-M.; Lim, S.; Lee, H. Direct Indium Tin Oxide Patterning Using Thermal Nanoimprint Lithography for Highly Efficient Optoelectronic Devices. *J. Vac. Sci. Technol., B* **2009**, *27*, 2786–2789.
83. Wiley, B. J.; Qin, D.; Xia, Y. Nanofabrication at High Throughput and Low Cost. *ACS Nano* **2010**, *4*, 3554–3559.
84. Vieu, C.; Carcenac, F.; Pepin, A.; Chen, Y.; Mejias, M.; Lebib, A.; Manin-Ferlazzo, L.; Couraud, L.; Launois, H. Electron Beam Lithography: Resolution Limits and Applications. *Appl. Surf. Sci.* **2000**, *164*, 111–117.
85. Hoff, J. D.; Cheng, L. J.; Meyhofer, E.; Guo, L. J.; Hunt, A. J. Nanoscale Protein Patterning by Imprint Lithography. *Nano Lett.* **2004**, *4*, 853–857.
86. Park, H. J.; Kang, M.-G.; Guo, L. J. Large Area High Density Sub-20 nm SiO_2 Nanostructures Fabricated by Block Copolymer Template for Nanoimprint Lithography. *ACS Nano* **2009**, *3*, 2601–2608.
87. Ji, S.; Liu, C.-C.; Liu, G.; Nealey, P. F. Molecular Transfer Printing Using Block Copolymers. *ACS Nano* **2009**, *4*, 599–609.
88. Tao, J. R.; Chen, Y. F.; Zhao, X. Z.; Malik, A.; Cui, Z. Room Temperature Nanoimprint Lithography Using a Bilayer of HSQ/PMMA Resist Stack. *Microelectron. Eng.* **2005**, *78−79*, 665–669.
89. Mele, E.; Di Benedetto, F.; Persano, L.; Cingolani, R.; Pisignano, D. Multilevel, Room-Temperature Nanoimprint Lithography for Conjugated Polymer-Based Photonics. *Nano Lett.* **2005**, *5*, 1915–1919.
90. Park, J. Y.; Hendricks, N. R.; Carter, K. R. Solvent-Assisted Soft Nanoimprint Lithography for Structured Bilayer Heterojunction Organic Solar Cells. *Langmuir* **2011**, *27*, 11251–11258.
91. Khang, D.-Y.; Kang, H.; Kim, T.-I.; Lee, H. H. Low-Pressure Nanoimprint Lithography. *Nano Lett.* **2004**, *4*, 633–637.
92. Cheng, X.; Guo, L. J.; Fu, P. F. Room-Temperature, Low-Pressure Nanoimprinting Based on Cationic Photopolymerization of Novel Epoxysilicone Monomers. *Adv. Mater.* **2005**, *17*, 1419–1424.
93. Lebib, A.; Chen, Y.; Cambril, E.; Youinou, P.; Studer, V.; Natali, M.; Pepin, A.; Janssen, H. M.; Sijbesma, R. P.

Room-Temperature and Low-Pressure Nanoimprint Lithography. *Microelectron. Eng.* **2002**, *61*−*62*, 371–377.
94. Ahn, S. H.; Guo, L. J. Large-Area Roll-to-Roll and Roll-to-Plate Nanoimprint Lithography: A Step toward High-Throughput Application of Continuous Nanoimprinting. *ACS Nano* **2009**, *3*, 2304–2310.
95. Stuart, C.; Chen, Y. Roll in and Roll Out: A Path to High-Throughput Nanoimprint Lithography. *ACS Nano* **2009**, *3*, 2062–2064.
96. Makela, T.; Haatainen, T.; Majander, P.; Ahopelto, J. Continuous Roll to Roll Nanoimprinting of Inherently Conducting Polyaniline. *Microelectron. Eng.* **2007**, *84*, 877–879.
97. Ahn, S. H.; Guo, L. J. Dynamic Nanoinscribing for Continuous and Seamless Metal and Polymer Nanogratings. *Nano Lett.* **2009**, *9*, 4392–4397.
98. Park, H. J.; Kang, M.-G.; Ahn, S. H.; Guo, L. J. A Facile Route to Polymer Solar Cells with Optimum Morphology Readily Applicable to a Roll-to-Roll Process without Sacrificing High Device Performance. *Adv. Mater.* **2010**, *22*, E247–E253.
99. Krebs, F. C. Polymer Solar Cell Modules Prepared Using Roll-to-Roll Methods: Knife-over-Edge Coating, Slot-Die Coating and Screen Printing. *Sol. Energy Mater. Sol. Cells* **2009**, *93*, 465–475.
100. Krebs, F. C.; Fyenbo, J.; Jorgensen, M. Product Integration of Compact Roll-to-Roll Processed Polymer Solar Cell Modules: Methods and Manufacture Using Flexographic Printing, Slot-Die Coating and Rotary Screen Printing. *J. Mater. Chem.* **2010**, *20*, 8994–9001.
101. Krebs, F. C.; Jorgensen, M.; Norrman, K.; Hagemann, O.; Alstrup, J.; Nielsen, T. D.; Fyenbo, J.; Larsen, K.; Kristensen, J. A Complete Process for Production of Flexible Large Area Polymer Solar Cells Entirely Using Screen Printing-First Public Demonstration. *Sol. Energy Mater. Sol. Cells* **2009**, *93*, 422–441.
102. Gaudiana, R. Third-Generation Photovoltaic Technology - The Potential for Low-Cost Solar Energy Conversion. *J. Phys. Chem. Lett.* **2010**, *1*, 1288–1289.
103. Tao, J. L.; Zhao, X. M.; Gao, J. M.; Hu, W. Lithographically Defined Uniform Worm-Shaped Polymeric Nanoparticles. *Nanotechnology* **2010**, *21*, 109802.
104. Tomohiro, K.; Hoto, N.; Kawata, H.; Hirai, Y. Fine Pattern Transfer of Functional Organic Polymers by Nanoimprint. *J. Photopolym. Sci. Technol.* **2011**, *24*, 71–75.
105. Keddie, J. L.; Jones, R. A. L.; Cory, R. A. Size-Dependent Depression of the Glass-Transition Temperature in Polymer-Films. *Europhys. Lett.* **1994**, *27*, 59–64.
106. Peet, J.; Wen, L.; Byrne, P.; Rodman, S.; Forberich, K.; Shao, Y.; Drolet, N.; Gaudiana, R.; Dennler, G.; Waller, D. Bulk Heterojunction Solar Cells with Thick Active Layers and High Fill Factors Enabled by a Bithiophene-*co*-Thiazolothiazole Push-Pull Copolymer. *Appl. Phys. Lett.* **2011**, *98*, 043301.
107. Shaheen, S. E.; Brabec, C. J.; Sariciftci, N. S.; Padinger, F.; Fromherz, T.; Hummelen, J. C. 2.5% Efficient Organic Plastic Solar Cells. *Appl. Phys. Lett.* **2001**, *78*, 841–843.
108. Melzer, C.; Koop, E. J.; Mihailetchi, V. D.; Blom, P. W. M. Hole Transport in Poly(phenylene vinylene)/Methanofullerene Bulk-Heterojunction Solar Cells. *Adv. Funct. Mater.* **2004**, *14*, 865–870.
109. Alvin, M. G.; Albert, R. Double Extraction of Uniformly Generated Electron - Hole Pairs from Insulators with Noninjecting Contacts. *J. Appl. Phys.* **1971**, *42*, 2823–2830.
110. Yang, J.; Nguyen, T.-Q. Effects of Thin Film Processing on Pentacene/C_{60} Bilayer Solar Cell Performance. *Org. Electron.* **2007**, *8*, 566–574.
111. Stevens, D. M.; Qin, Y.; Hillmyer, M. A.; Frisbie, C. D. Enhancement of the Morphology and Open Circuit Voltage in Bilayer Polymer/Fullerene Solar Cells. *J. Phys. Chem. C* **2009**, *113*, 11408–11415.
112. Kim, K.; Liu, J. W.; Carroll, D. L. Thermal Diffusion Processes in Bulk Heterojunction Formation for Poly-3-hexylthiophene/C_{60} Single Heterojunction Photovoltaics. *Appl. Phys. Lett.* **2006**, *88*, 181911.
113. Geiser, A.; Fan, B.; Benmansour, H.; Castro, F.; Heier, J.; Keller, B.; Mayerhofer, K. E.; Nueesch, F.; Hany, R. Poly(3-hexylthiophene)/C_{60} Heterojunction Solar Cells: Implication of Morphology on Performance and Ambipolar Charge Collection. *Sol. Energy Mater. Sol. Cells* **2008**, *92*, 464–473.
114. Lee, K. H.; Schwenn, P. E.; Smith, A. R. G.; Cavaye, H.; Shaw, P. E.; James, M.; Krueger, K. B.; Gentle, I. R.; Meredith, P.; Burn, P. L. Morphology of All-Solution-Processed "Bilayer" Organic Solar Cells. *Adv. Mater.* **2011**, *23*, 766–770.
115. Yan, H.; Swaraj, S.; Wang, C.; Hwang, I.; Greenham, N. C.; Groves, C.; Ade, H.; McNeill, C. R. Influence of Annealing and Interfacial Roughness on the Performance of Bilayer Donor/Acceptor Polymer Photovoltaic Devices. *Adv. Funct. Mater.* **2010**, *20*, 4329–4337.